APPENDIX
Replacement of the calculated structure factor amplitude by the experimental one

When for a reflection the exact value of the structure factor amplitude F^o is known and there is a 'calculated' value of the structure factor $F^c \exp(i\varphi^c)$, common practice is to use the 'mixed' value of the structure factor $F^o \exp(i\varphi^c)$ for further calculation.

It can be seen that the value $F^o \exp(i\varphi^c)$ is more exact than $F^c \exp(i\varphi^c)$ only when

$$F^c/F^o > 1, \text{ or when } F^c/F^o < 1 - 4\sin^2(\Delta\varphi/2).$$

Here $\Delta\varphi$ is the error in the calculation of phase φ^c.

In particular, if $\Delta\varphi > \pi/3$, then for all $F^c < F^o$ the value $F^o \exp(i\varphi^c)$ is less exact than $F^c \exp(i\varphi^c)$. This is why we must be careful in ascribing to the observed amplitude the calculated phase when F^c is smaller than F^o.

References

BUKVETSKAYA, L. V., SHISHOVA, T. G., ANDRIANOV, V. I. & SIMONOV, V. I. (1977). *Kristallografiya*, **22**, 494-497.

DAVIES, A. R. & ROLLETT, J. S. (1976). *Acta Cryst.* A**23**, 17-23.

NAVAZA, J., CASTELLANO, E. E. & TSOUCARIS, G. (1983). *Acta Cryst.* A**39**, 622-631.

QURASHI, M. M. (1953). *Acta Cryst.* **6**, 103.

RANGO, C. DE, TSOUCARIS, G. & ZELWER, C. (1969). *Acta Cryst.* A**25**, S85.

SIROTA, M. I. & SIMONOV, V. I. (1970). *Kristallografiya*, **15**, 681-685.

VAINSTEIN, B. K. & KHACHATURYAN, A. G. (1977). *Kristallografiya*, **22**, 706-710.

Acta Cryst. (1988). A**44**, 150-157

Wide-Angle X-ray Diffraction of Materials Comprising Layer-Type Molecules

BY M. SHIOYA AND A. TAKAKU

Department of Textile and Polymeric Materials, Tokyo Institute of Technology, O-okayama, Meguro-ku, Tokyo, Japan

(*Received* 9 *January* 1987; *accepted* 1 *October* 1987)

Abstract

The shapes of the wide-angle X-ray reflexion profiles produced by materials comprising layer-type molecules, such as carbon fibres and pyrolytic graphites, are affected by distortions, sizes and preferential orientation of the crystallites. In the present study, the diffraction intensity distribution of layer-type materials has been deduced theoretically as a function of structural parameters and measuring direction. The reflexion profiles of carbon fibres have been simulated to investigate the effects of structural parameters on the modulation of the diffraction pattern.

1. Introduction

The crystallites in non-graphitic carbons such as carbon fibres and pyrolytic graphites are parallel stacks of individual graphite layers with no regularity of packing in mutual translations parallel to the layer. The wide-angle X-ray diffraction patterns of layer-type materials of this kind show 00*l* and *hk* reflexions, but do not exhibit general *hkl* reflexions. The *hk* reflexion profiles resulting from a random orientation of randomly stacked layers of finite size were first analysed by Warren (1941).

The *hk* reflexions are strongly asymmetric, and this peculiar peak shape is affected by preferential orientation of the crystallites. Guentert & Cvikevich (1964) have given a method to convert the *hk* reflexion profiles caused by randomly stacked layers of infinite size with preferential orientation into those with random orientation. Ruland & Tompa (1968, 1972) have expressed the *hk* reflexion profiles of randomly stacked layers as a function of the layer size and the degree of preferential orientation.

In certain layer-type carbons, there exists some degree of regularity in mutual translations of neighbouring layers (Franklin, 1951; Ruland, 1965; Fischer & Ruland, 1980). With increasing regularity, the asymmetric *hk* reflexions turn into the symmetric *hkl* reflexions (Houska & Warren, 1954). Ruland (1965) has evaluated the degree of regularity for powder samples of graphitic carbons.

This study analyses the wide-angle X-ray diffraction by finite-size crystallites with preferential orientation, comprising layer-type molecules stacked with Hosemann distortions of the second kind. The results of this study form the basis of trial-and-error evaluation of structural parameters. In the following discussion, the structure of layer-type materials is expressed by the electron density distribution. Then,

0108-7673/88/020150-08$03.00

the diffraction intensity distribution from a crystallite and material are deduced. Finally, the reflexion profiles are computed in order to show modulations of the diffraction pattern.

Although layer-type carbons are analysed as a typical example, the mathematical treatment developed in this study is applicable to layer-type materials in general.

2. Structure of material

The structural elements comprising layer-type carbons are C atoms, two-dimensional unit cells, lattice layers, layer sets and stacks of layer sets. We shall define the density distribution function, which is the number per unit volume of origins of elements existing at a position $\mathbf{x}$ from the origin of one rank higher-order element, as follows.

$\rho_a(\mathbf{x})$: distribution of electrons in an atom.
$\rho_u(\mathbf{x})$: distribution of atoms in a unit cell.
$\rho_l(\mathbf{x})$: distribution of unit cells in a lattice layer.
$\rho_s(\mathbf{x})$: distribution of lattice layers in a layer set.
$\rho_c(\mathbf{x})$: distribution of layer sets in a stack of layer sets.

Let us consider the electron density distribution of a unit cell. The number of atoms encountered in a volume element dv_y at a position $\mathbf{y}$ from the origin of unit cell is $\rho_u(\mathbf{y})\,dv_y$. Among the electrons belonging to an atom at a position $\mathbf{y}$, the number per unit volume of those existing at a position $\mathbf{x}$ is $\rho_a(\mathbf{x}-\mathbf{y})$. Therefore, we find that, among the electrons belonging to all the atoms in this unit cell, the number per unit volume of those existing at a position $\mathbf{x}$ is given by $\int \rho_u(\mathbf{y})\rho_a(\mathbf{x}-\mathbf{y})\,dv_y$. That is, the electron density distribution of a unit cell is given by the convolution of $\rho_u(\mathbf{x})$ and $\rho_a(\mathbf{x})$. Similarly, the electron density distribution of a crystallite, $\rho(\mathbf{x})$, is given by the convolution of $\rho_c(\mathbf{x})$, $\rho_s(\mathbf{x})$, $\rho_l(\mathbf{x})$, $\rho_u(\mathbf{x})$ and $\rho_a(\mathbf{x})$.

In a unit cell, two C atoms are situated respectively at positions $\mathbf{x}=\mathbf{0}$ and $\mathbf{x}=2\mathbf{a}/3+\mathbf{b}/3$, where $\mathbf{a}$ and $\mathbf{b}$ are the vectors representing the periods of repetition of unit cells. The lattice layer comprises the unit-cell repetitions N_a and N_b times in the respective directions of $\mathbf{a}$ and $\mathbf{b}$. In a layer set, two lattice layers are located at positions $\mathbf{x}=\mathbf{0}$ and $\mathbf{x}=\mathbf{y}$. The position $\mathbf{y}$ distributes statistically around $\mathbf{x}=\mathbf{a}/3+2\mathbf{b}/3+\mathbf{c}/2$ with the probability distribution expressed as $\delta[\mathbf{y}-(\mathbf{a}/3+2\mathbf{b}/3+\mathbf{c}/2)]*D(\mathbf{y})$, where $\mathbf{c}$ is the vector representing the average period of repetition of layer sets, $D(\mathbf{y})$ the probability distribution function with average $\mathbf{y}=\mathbf{0}$, $\delta(\mathbf{y})$ the Dirac delta function, and $*$ convolution. The convolution $\delta(\mathbf{y}-\mathbf{y}_0)*f(\mathbf{y})$ corresponds to the function $f(\mathbf{y})$ translated by a vector $\mathbf{y}_0$ [see (48)].

In a crystallite, N_c layer sets are stacked with Hosemann distortion of the second kind. Here, the distortions of the second kind mean that the arrangement of elements is defined statistically by the probability distribution of spacing between nearest-neighbouring elements (Bonart, Hosemann & McCullough, 1963). We shall number the lattice layers in a crystallite in the order of arrangement. Then, for hexagonal-type packing, the probability distribution of spacing between the nth and $(n+1)$th layers is expressed as $\delta[\mathbf{x}-(\mathbf{a}/3+2\mathbf{b}/3+\mathbf{c}/2)]*D(\mathbf{x})$, and that of spacing between the $(n+1)$th and $(n+2)$th layers is shown as $\delta[\mathbf{x}-(-\mathbf{a}/3-2\mathbf{b}/3+\mathbf{c}/2)]*D(\mathbf{x})$. Therefore, the probability distribution of spacing between the nth and $(n+2)$th layers is given by the convolution of the above two probability distributions, that is, $\delta(\mathbf{x}-\mathbf{c})*D(\mathbf{x})*D(\mathbf{x})$ [see (46)-(48)]. This convolution is equivalent to the probability distribution of spacing between nearest-neighbouring layer sets.

We now number the layer sets in the order of arrangement. Then, the probability distribution of spacing between the nth and $(n+2)$th layer sets is given by the convolution of two $\delta(\mathbf{x}-\mathbf{c})*D(\mathbf{x})*D(\mathbf{x})$'s and that of spacing between the nth and $(n+3)$th layer sets is given by the convolution of three $\delta(\mathbf{x}-\mathbf{c})*D(\mathbf{x})*D(\mathbf{x})$'s. Therefore, the probability distribution of spacing between the nth and $(n+m)$th layer sets is generally given by the convolution of m $\delta(\mathbf{x}-\mathbf{c})*D(\mathbf{x})*D(\mathbf{x})$'s. The probability distribution of spacing between the nth and $(n-m)$th layer sets is given by the convolution of m $\delta(-\mathbf{x}-\mathbf{c})*D(-\mathbf{x})*D(-\mathbf{x})$'s. The probability distribution of spacing between a layer set and this layer set itself is given by $\delta(\mathbf{x})$. In consequence, the probability distribution of spacing between layer sets is given by the multiple convolution of $\delta(\mathbf{x}-\mathbf{c})*D(\mathbf{x})*D(\mathbf{x})$'s, or of $\delta(-\mathbf{x}-\mathbf{c})*D(-\mathbf{x})*D(-\mathbf{x})$'s, or $\delta(\mathbf{x})$.

The function $\rho_c(\mathbf{x})$ is related to these probability distributions by the form of $\rho_c(\mathbf{x})*\rho_c(-\mathbf{x})$. If the position of the nth layer set is denoted as $\mathbf{x}_n$, $\rho_c(\mathbf{x})$ is represented as $\sum_{n=1}^{N_c}\delta(\mathbf{x}-\mathbf{x}_n)$, and thus $\rho_c(\mathbf{x})*\rho_c(-\mathbf{x})$ becomes $\rho_c(\mathbf{x})*\sum_{n=1}^{N_c}\delta(-\mathbf{x}-\mathbf{x}_n)$. By considering the relation $\delta(-\mathbf{x})=\delta(\mathbf{x})$ and using (48), we find that $\rho_c(\mathbf{x})*\rho_c(-\mathbf{x})=\sum_{n=1}^{N_c}\rho_c(\mathbf{x}+\mathbf{x}_n)$. The density distribution $\rho_c(\mathbf{x}+\mathbf{x}_n)$ is the translation of $\rho_c(\mathbf{x})$ by the vector $-\mathbf{x}_n$, and represents the density distribution of layer sets when the origin of the distribution is located at the position of the nth layer set. The terminal points of a fixed vector $\mathbf{x}$ from some layer sets are situated outside the crystallite. We shall assign the numbers from $N_i(\mathbf{x})+1$ to N_c to these layer sets. Then, $\rho_c(\mathbf{x}+\mathbf{x}_n)$ becomes 0 for the layer sets with $N_i(\mathbf{x})+1\le n\le N_c$. For the remaining layer sets, $\sum_{n=1}^{N_i}\rho_c(\mathbf{x}+\mathbf{x}_n)$ is expressed as $N_i(\mathbf{x})\langle\rho_c(\mathbf{x}+\mathbf{x}_n)\rangle$, where $\langle\ \rangle$ stands for the average over the layer sets with $1\le n\le N_i(\mathbf{x})$. The average $\langle\rho_c(\mathbf{x}+\mathbf{x}_n)\rangle$ is given by the sum of the multiple convolutions of $\delta(\mathbf{x}-\mathbf{c})*D(\mathbf{x})*D(\mathbf{x})$'s and of $\delta(-\mathbf{x}-\mathbf{c})*D(-\mathbf{x})*D(-\mathbf{x})$'s, and $\delta(\mathbf{x})$.

The structure mentioned above is therefore written in the mathematical expressions as follows.

$$\rho(\mathbf{x}) = \rho_c(\mathbf{x}) * \rho_s(\mathbf{x}) * \rho_l(\mathbf{x}) * \rho_u(\mathbf{x}) * \rho_a(\mathbf{x}). \quad (1)$$

$$\rho_u(\mathbf{x}) = \delta(\mathbf{x}) + \delta[\mathbf{x} - (2\mathbf{a}/3 + \mathbf{b}/3)]. \quad (2)$$

$$\rho_l(\mathbf{x}) = \sum_{m=0}^{N_a-1} \sum_{n=0}^{N_b-1} \delta[\mathbf{x} - (m\mathbf{a} + n\mathbf{b})]. \quad (3)$$

$$\rho_s(\mathbf{x}) = \delta(\mathbf{x}) + \delta(\mathbf{x} - \mathbf{y}), \quad (4)$$

where $\mathbf{y}$ distributes statistically according to the function $\delta[\mathbf{y} - (\mathbf{a}/3 + 2\mathbf{b}/3 + \mathbf{c}/2)] * D(\mathbf{y})$.

$$\rho_c(\mathbf{x}) * \rho_c(-\mathbf{x}) = N_i(\mathbf{x})\{\delta(\mathbf{x}) + \sum_{n=1}^{\infty} [\delta(\mathbf{x} - \mathbf{c}) * D(\mathbf{x}) * D(\mathbf{x})]^{*n} + \sum_{n=1}^{\infty} [\delta(-\mathbf{x} - \mathbf{c}) * D(-\mathbf{x}) * D(-\mathbf{x})]^{*n}\}, \quad (5)$$

by letting $\mathbf{x} = p\mathbf{a} + q\mathbf{b} + r\mathbf{c}$,

$$N_i(\mathbf{x}) = \begin{cases} N_c - |r| & (|r| \le N_c) \\ 0 & (|r| \ge N_c). \end{cases} \quad (6)$$

The notations $*$ and $*^n$ stand for convolution and multiple convolution, respectively, defined as

$$f(\mathbf{x}) * g(\mathbf{x}) = \int f(\mathbf{y}) g(\mathbf{x} - \mathbf{y})\, \mathrm{d}v_y \quad (7)$$

and

$$f(\mathbf{x})^{*n} = [f(\mathbf{x})^{*(n-1)}] * f(\mathbf{x}), \quad f(\mathbf{x})^{*0} = \delta(\mathbf{x}). \quad (8)$$

In the material, N_0 crystallites are assembled with preferential orientation. Denote the reciprocal vectors of $\mathbf{a}$, $\mathbf{b}$ and $\mathbf{c}$ as $\mathbf{a}^*$, $\mathbf{b}^*$ and $\mathbf{c}^*$. The reciprocal vector $\mathbf{c}$ is perpendicular to the layer plane [see (66)]. Thus, the orientation of a crystallite is specified by the directions of $\mathbf{c}$ and $\mathbf{a}$. We shall define the angles φ, ξ and τ between the vectors, and the angles ε, η and μ between planes, as shown in Fig. 1. As the primary axis, it is preferable to chose the fibre axis in the case of fibres, or the perpendicular of the plane of deposition in the case of pyrolytic carbons. The directions of $\mathbf{c}^*$ and $\mathbf{a}$ are then specified by ε, ξ and μ. Therefore, preferential orientation of the crystallites is expressed by the orientation distribution function $P(\varepsilon, \xi, \mu)$, which is normalized so that

$$\int_{\varepsilon=0}^{2\pi} \int_{\xi=0}^{\pi} \int_{\mu=0}^{2\pi} P(\varepsilon, \xi, \mu) \sin \xi\, \mathrm{d}\mu\, \mathrm{d}\xi\, \mathrm{d}\varepsilon = 1. \quad (9)$$

As for carbon fibres, P is well represented by the equation

$$P(\xi) = \Gamma[(w+3)/2]/\{4\pi^{5/2}\Gamma[(w+2)/2]\} \sin^w \xi, \quad (10)$$

where $\Gamma(x)$ is the gamma function, and w is related to $\Delta\xi$, the half maximum width of $P(\xi)$, as

$$w = -\ln 2/\ln[\cos(\Delta\xi/2)]. \quad (11)$$

Since $\sin\xi\, \mathrm{d}\xi\, \mathrm{d}\varepsilon = \sin\tau\, \mathrm{d}\tau\, \mathrm{d}\eta$, $\mathrm{d}N$, the number of the crystallites included in the region $\mu - \mu + \mathrm{d}\mu$, $\tau - \tau + \mathrm{d}\tau$ and $\eta - \eta + \mathrm{d}\eta$ is given as

$$\mathrm{d}N = N_0 P(\varepsilon, \xi, \mu) \sin\tau\, \mathrm{d}\mu\, \mathrm{d}\tau\, \mathrm{d}\eta, \quad (12)$$

where ξ and ε are related to τ and η by the spherical trigonometry as

$$\cos\xi = \cos\varphi \cos\tau + \sin\varphi \sin\tau \cos\eta \quad (13)$$

and

$$\cos\tau = \cos\varphi \cos\xi + \sin\varphi \sin\xi \cos\varepsilon. \quad (14)$$

The basic relationships often used in this study are summarized in Appendix § 1.

3. Diffraction by crystallite

The X-ray diffraction intensity of a crystallite, $I_c(\mathbf{s})$, is given as

$$I_c(\mathbf{s}) = |\mathscr{F}(\rho(\mathbf{x}))|^2 I_e(\mathbf{s}), \quad (15)$$

where

$$\mathbf{s} = (\mathbf{s}_d - \mathbf{s}_i)/\lambda \quad (16)$$

and $\mathbf{s}_d$ and $\mathbf{s}_i$ are the unit vectors parallel to the diffracted and incident beams, respectively, λ the X-ray wavelength, $I_e(\mathbf{s})$ the diffraction intensity of one electron, and $\mathscr{F}$ the Fourier transform defined as

$$\mathscr{F}[f(\mathbf{x})] = \int f(\mathbf{x}) \exp[-2\pi i \mathbf{s}.\mathbf{x}]\, \mathrm{d}v_x. \quad (17)$$

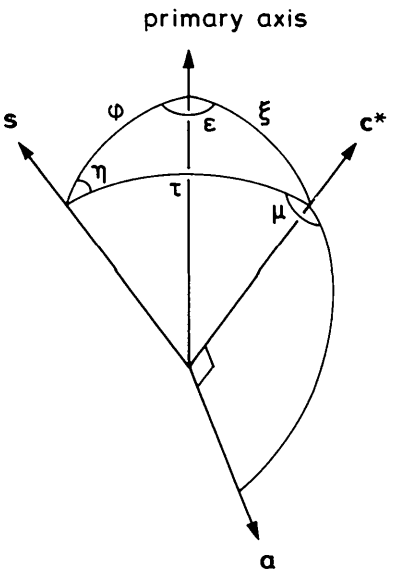

Fig. 1. Geometrical relationships of the primary axis, $\mathbf{s}$, $\mathbf{c}^*$ and $\mathbf{a}$.

The vector **s** is represented by the linear combination of **a***, **b*** and **c*** as

$$\mathbf{s} = h\mathbf{a}^* + k\mathbf{b}^* + l\mathbf{c}^*. \tag{18}$$

The absolute value of **s** is $2(\sin\theta)/\lambda$, where 2θ is the diffraction angle. Substitution of (1) into (15) gives

$$I_c = |\mathscr{F}(\rho_c)|^2|\mathscr{F}(\rho_s)|^2|\mathscr{F}(\rho_l)|^2|\mathscr{F}(\rho_u)|^2 \times |\mathscr{F}(\rho_a)|^2 I_e. \tag{19}$$

In (19), I_e is given by the Thomson theory, $\mathscr{F}(\rho_a)$ is the atomic scattering factor, and $|\mathscr{F}(\rho_u)|$ and $|\mathscr{F}(\rho_l)|$ are calculated using (2) and (3), respectively. By taking account of the statistical distribution of the positions of respective layers in a layer set, $\mathscr{F}(\rho_s)$ is approximated by the average of $\mathscr{F}(\rho_s)$ given by the equation (see Appendix § 2)

$$\mathscr{F}(\rho_s) \simeq \int \mathscr{F}(\rho_s)\delta[\mathbf{y} - (\mathbf{a}/3 + 2\mathbf{b}/3 + \mathbf{c}/2)] * D(\mathbf{y})\, \mathrm{d}v_y. \tag{20}$$

The function $|\mathscr{F}(\rho_c)|^2$ is obtained by the Fourier transform of $\rho_c(\mathbf{x}) * \rho_c(-\mathbf{x})$ (see Appendix § 3).

Consequently, each term in (19) takes the form

$$I_e = e^4 I_i(1 + \cos^2 2\theta)/(2m^2c^4L^2) \tag{21}$$

$$\mathscr{F}(\rho_a) = 4{\cdot}47 \exp[-0{\cdot}04528nm^2|\mathbf{s}|^2] + 1{\cdot}53 \tag{22}$$

$$|\mathscr{F}(\rho_u)|^2 = 2 + 2\cos[2\pi(2h/3 + k/3)] \tag{23}$$

$$|\mathscr{F}(\rho_l)|^2 = \sum_{h_0}\sum_{k_0} N_a^2 N_b^2 \exp\{-\pi[N_a^2(h-h_0)^2 + N_b^2(k-k_0)^2]\} \tag{24}$$

$$|\mathscr{F}(\rho_s)|^2 = 1 + R^2 + 2R\cos\{2\pi[h/3 + 2k/3 + l/2 - \zeta]\} \tag{25}$$

and

$$|\mathscr{F}(\rho_c)|^2 = L_c/|\mathbf{c}|\Big\{\sum_{l_0} 2R^2 L_c/\{(1+R^2) \times [|\mathbf{c}|^2 + (1-R^2)^2 L_c^2/4]^{1/2}\} \times \exp\{-\pi L_c^2(l - l_0 - 2\zeta)^2/[|\mathbf{c}|^2 + (1-R^2)^2 L_c^2/4]\} + (1-R^2)/(1+R^2)\Big\}, \tag{26}$$

where e is the elementary electric charge, m the electron mass, c the light velocity, L the sample-to-receiver distance, I_i the intensity of the incident beam, and L_c the stacking height of a crystallite represented as

$$L_c = N_c|\mathbf{c}|. \tag{27}$$

The parameters R and ζ are the functions of h, k and l, and represent respectively the absolute value and the phase factor of the Fourier transform of $D(\mathbf{x})$,

$$\mathscr{F}[D(\mathbf{x})] = R\exp[2\pi i\zeta]. \tag{28}$$

The regularity of stacking can be evaluated by R. From (57), it is known that in any case R satisfies the relation

$$0 \le R \le 1. \tag{29}$$

For a crystallite with complete three-dimensional regularity, $R = 1$, and for randomly stacked layers, $R = 0$. If $D(-\mathbf{x}) = D(\mathbf{x})$, as is the case with Gaussian distribution, then $\zeta = 0$.

4. Diffraction by materials

Since the diffraction intensity of a material, $I(\mathbf{s})$, is the sum of the diffraction intensity of crystallites, we have

$$I(\mathbf{s}) = \int I_c(\mathbf{s})\, \mathrm{d}N. \tag{30}$$

Substitution of (12) and (19) into (30) yields

$$I = \int_{\eta=0}^{2\pi}\int_{\tau=0}^{\pi}\int_{\mu=0}^{2\pi} N_0|\mathscr{F}(\rho_c)|^2|\mathscr{F}(\rho_s)|^2|\mathscr{F}(\rho_l)|^2 \times |\mathscr{F}(\rho_u)|^2|\mathscr{F}(\rho_a)|^2 I_e P \sin\tau\, \mathrm{d}\mu\, \mathrm{d}\tau\, \mathrm{d}\eta. \tag{31}$$

We shall define the angles between **a** and **b**, **b** and **c**, **c** and **a** as γ, α, β, respectively. The spherical trigonometry gives the cosines of the angles between **a** and **s**, **b** and **s**, **c*** and **s** as $\sin\tau\cos\mu$, $\sin\tau\cos(\mu+\gamma)$, $\cos\tau$, respectively. Thus the calculations of the inner products of **s** and **a**, **s** and **b**, **s** and **c*** by using (18) yield

$$h = |\mathbf{s}||\mathbf{a}|\sin\tau\cos\mu, \tag{32}$$

$$k = |\mathbf{s}||\mathbf{b}|\sin\tau\cos(\mu+\gamma) \tag{33}$$

and

$$l = |\mathbf{s}||\mathbf{c}|\sin^{-1}\gamma\{v\cos\tau/(|\mathbf{a}||\mathbf{b}||\mathbf{c}|) + \sin\tau[\cos\beta\sin(\mu+\gamma) - \cos\alpha\sin\mu]\}, \tag{34}$$

where v is the volume of the parallelepiped having **a**, **b**, **c** as adjacent edges. Equation (31) is the general conclusion of the wide-angle X-ray diffraction intensity of layer-type materials.

Provided that P is independent of μ, and that $\alpha = \beta = \pi/2$, as is the case with layer-type carbons, (31) can be further simplified when $(h_0\, k_0) \neq (0\,0)$. In this case, the μ-dependent functions in the integrand of (31) are $|\mathscr{F}(\rho_s)|^2$, $|\mathscr{F}(\rho_l)|^2$, $|\mathscr{F}(\rho_u)|^2$, R and ζ. We shall denote the values of $|\mathbf{s}|$, τ and μ when $(h\,k\,l) = (h_0\, k_0\, l_0)$ as $|\mathbf{s}|_0$, τ_0 and μ_0, respectively. Since $|\mathscr{F}(\rho_l)|^2$ takes a large value only in the vicinity of $\mu = \mu_0$, μ in $|\mathscr{F}(\rho_s)|^2$, $|\mathscr{F}(\rho_u)|^2$, R and ζ may be approximated by μ_0. Then these functions can be removed from the integration concerning μ. The Taylor series of $\cos\mu$ and $\cos(\mu+\gamma)$ around $\mu = \mu_0$ give

$$h - h_0 \simeq -|\mathbf{s}|\sin\tau|\mathbf{a}|\sin\mu_0(\mu - \mu_0) + (|\mathbf{s}|\sin\tau - |\mathbf{s}|_0\sin\tau_0)|\mathbf{a}|\cos\mu_0$$

and

$$k-k_0 \simeq -|\mathbf{s}| \sin \tau |\mathbf{b}| \sin (\mu_0+\gamma)(\mu-\mu_0) + (|\mathbf{s}| \sin \tau - |\mathbf{s}|_0 \sin \tau_0)|\mathbf{b}| \cos (\mu_0+\gamma).$$

After substitution of the above expressions into $|\mathscr{F}(\rho_l)|^2$, the integration of $\int |\mathscr{F}(\rho_l)|^2 \, d\mu$ is calculated by expanding the integration to the region $-\infty < \mu < \infty$. The summations $\sum_{h_0} \sum_{k_0}$ are removed from the integrations concerning η and τ.

It is concluded that the diffraction intensity of layer-type carbons with $(h_0\, k_0) \neq (0\, 0)$ is given by the equation

$$I = \sum_{h_0} \sum_{k_0} N_0 |\mathscr{F}(\rho_a)|^2 I_e \int_{\tau=0}^{\pi} |\mathscr{F}(\rho_c)|^2 |\mathscr{F}(\rho_s)|^2 + \int |\mathscr{F}(\rho_l)|^2 \, d\mu |\mathscr{F}(\rho_u)|^2 \int_{\eta=0}^{2\pi} P(\varepsilon, \xi) \, d\eta \sin \tau \, d\tau, \quad (35)$$

where

$$|\mathscr{F}(\rho_u)|^2 = 2 + 2 \cos \{2\pi[2h_1/3 + k_1/3]\}, \quad (36)$$

$$\int |\mathscr{F}(\rho_l)|^2 \, d\mu = VL_a|\mathbf{c}|^2/(L_c v^2 |\mathbf{s}| \sin \tau) \times \exp [-\pi L_a^2 (|\mathbf{s}| \sin \tau - |\mathbf{s}|_0 \sin \tau_0)^2], \quad (37)$$

$$|\mathscr{F}(\rho_s)|^2 = 1 + R^2 + 2R \times \cos \{2\pi[h_1/3 + 2k_1/3 + l/2 - \zeta]\} \quad (38)$$

$$R \exp [2\pi i\zeta] = R(h_1, k_1, l) \times \exp [2\pi i \zeta(h_1, k_1, l)], \quad (39)$$

$$h_1 = |\mathbf{s}| \sin \tau h_0/(|\mathbf{s}|_0 \sin \tau_0) \quad (40)$$

$$k_1 = |\mathbf{s}| \sin \tau k_0/(|\mathbf{s}|_0 \sin \tau_0) \quad (41)$$

and

$$|\mathbf{s}|_0 \sin \tau_0 = (\mathbf{h}_0^2/|\mathbf{a}|^2 + k_0^2/|\mathbf{b}|^2 - 2h_0 k_0 \cos \gamma/|\mathbf{a}||\mathbf{b}|)^{1/2}/\sin \gamma. \quad (42)$$

The parameter L_a represents the layer size defined as

$$1/L_a^2 = \sin^2 \mu_0/(N_b|\mathbf{b}| \sin \gamma)^2 + \sin^2 (\mu_0+\gamma)/(N_a|\mathbf{a}| \sin \gamma)^2. \quad (43)$$

V stands for the volume of one crystallite.

5. Computation of diffraction profiles

In this section, the effects of the structural parameters on the modulation of the $h\,k$ reflexion profiles of carbon fibres are investigated numerically on the basis of (35). The distribution profiles in the form of $I(\mathbf{s})/I_i$ for the 110 and 112 reflexions were computed with various values of R, L_a, $\Delta\zeta$ and φ, where the values used for the parameters without specifications are as follows: $|\mathbf{a}| = |\mathbf{b}| = 2{\cdot}461$, $|\mathbf{c}| = 6{\cdot}707$ Å (Ruland, 1968), $\gamma = 2\pi/3$ rad, $\zeta = 0$, $R = 0{\cdot}5$ (independent of h_1, k_1 and l), $L_a = 50$ Å, $L_c = 50$ Å, $\Delta\xi = 30°$, $\varphi = 0°$ (meridional reflexions), $h_0 = k_0 = 1$, $-3 \leq l_0 \leq 3$, $\lambda = 1{\cdot}542$ Å (Cu $K\alpha$ radiation), $N_0 V = 1$ mm^3 and $L = 100$ mm. The results of computations are shown in Figs. 2 to 5.

When $R = 1$, the 110 and 112 reflexion peaks appear at about $2\theta = 78$ and 84°, respectively (Fig. 2). The peak intensity ratio of the 112 reflexion to the 110 reflexion decreases with decreasing R, and becomes 0 when $R = 0$. Simultaneously, the 110 reflexion moves towards higher angles, and becomes asymmetric.

The layer size affects the sharpness of the reflexion peak (Fig. 3). The decrease in layer size makes the reflexion peaks broader.

The degree of preferential orientation and the measuring direction change the peak intensity ratio of the 112 and 110 reflexions (Figs. 4 and 5). For the three curves in Fig. 5, the peak intensity ratio takes the largest value when $\varphi = 45°$.

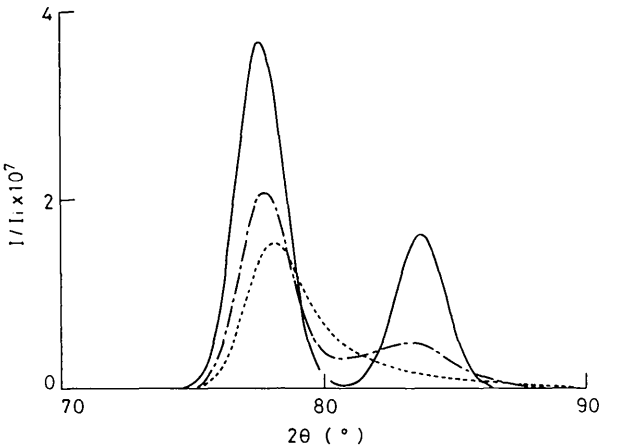

Fig. 2. 110 and 112 reflexion profiles of carbon fibres with $R = 0$ (- - -), $R = 0{\cdot}5$ (— — —) and $R = 1$ (——).

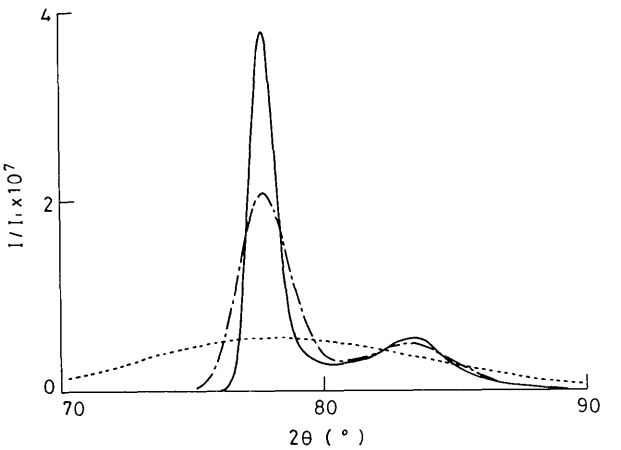

Fig. 3. 110 and 112 reflexion profiles of carbon fibres with L_a = 10 Å (- - -), $L_a = 50$ Å (— — —) and $L_a = 100$ Å (——).

6. Discussion

The inter-layer spacing of layer carbons exhibits generally a larger value than that of the graphite crystallite, 3·35 Å. From this, it can be considered that in a crystallite of layer carbons the inter-layer spacing shows a skewed distribution having a long tail at larger inter-layer spacings. Hence, in this section, we shall investigate how the parameters R and ζ for the $00l$ reflexions are affected by the type of the distribution function $D(\mathbf{x})$.

By defining the one-dimensional Fourier transform $\mathscr{F}_{sy}$ as

$$\mathscr{F}_{sy}[f(y)] = \int_{-\infty}^{\infty} f(y) \exp(-2\pi i s y)\, dy$$

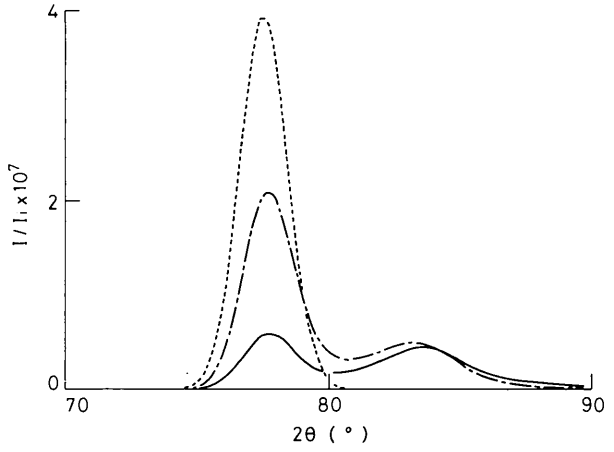

Fig. 4. 110 and 112 reflexion profiles of carbon fibres with $\Delta\xi = 0°$ (---), $\Delta\xi = 30°$ (— — —) and random orientation (——). The intensities with $\Delta\xi = 0°$ have been multiplied by a factor 0·4.

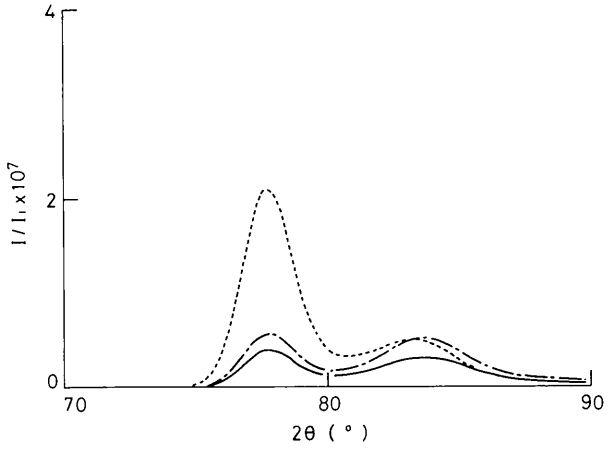

Fig. 5. 110 and 112 reflexion profiles of carbon fibres with $\varphi = 0°$ (---), $\varphi = 45°$ (— — —) and $\varphi = 90°$ (——).

and assuming that $D(\mathbf{x})$ is expressed as

$$D(\mathbf{x}) = \frac{1}{v} D_a(p) D_b(q) D_c(r),$$

where

$$\mathbf{x} = p\mathbf{a} + q\mathbf{b} + r\mathbf{c},$$

we obtain the equation

$$\mathscr{F}[D(\mathbf{x})] = \mathscr{F}_{hP}[D_a(p)]\mathscr{F}_{kq}[D_b(q)]\mathscr{F}_{lr}[D_c(r)].$$

When $h = k = 0$, we have

$$\mathscr{F}_{hP}[D_a(p)] = \mathscr{F}_{kq}[D_b(q)] = 1.$$

In the case that $D_c(r)$ is given by the Gaussian function as

$$D_c(r) = (\sqrt{2\pi}\sigma_c)^{-1} \exp[-r^2/2\sigma_c^2],$$

we have

$$\mathscr{F}_{lr}[D_c(r)] = \exp(-2\pi^2\sigma_c^2 l^2).$$

In the case that $D_c(r)$ is given by an asymmetric function as

$$D_c(r) = \begin{cases} (e\sigma_c)^{-1} \exp[-r/\sigma_c] & (r \geq -\sigma_c) \\ 0 & (r < -\sigma_c), \end{cases}$$

we have

$$\mathscr{F}_{lr}[D_c(r)] = (4\pi^2\sigma_c^2 l^2 + 1)^{-1/2} \times \exp[2\pi i \sigma_c l - i \arctan(2\pi\sigma_c l)].$$

In the above equations, σ_c stands for the standard deviation of r.

When σ_c is small, the general relationship between $\mathscr{F}_{lr}[D_c(r)]$ and σ_c is obtained. Whatever type $D_c(r)$ may be, it is expressed as

$$D_c(r) = \sigma_c^{-1} F(r/\sigma_c),$$

where $F(r)$ is a probability distribution function with average $r = 0$ and standard deviation 1. Thus, we obtain

$$\mathscr{F}_{lr}[D_c(r)] = \int_{-\infty}^{\infty} F(y) \exp[-2\pi i(\sigma_c l)y]\, dy.$$

The Taylor expansion of the right-hand side of the above equation concerning $\sigma_c l$ gives

$$\mathscr{F}_{lr}[D_c(r)] \simeq 1 - 2\pi^2\sigma_c^2 l^2 + (4/3)\pi^3 \left\{ \int_{-\infty}^{\infty} r^3 D_c(r)\, dr \right\} i l^3.$$

R and ζ are given as

$$R \simeq 1 - 2\pi^2\sigma_c^2 l^2, \tag{44}$$

$$\zeta \simeq (2/3)\pi^2 \left\{ \int_{-\infty}^{\infty} r^3 D_c(r)\, dr \right\} l^3. \tag{45}$$

These relationships are valid for any kind of distribution function $D_c(r)$ when $h = k = 0$ and σ_c is small.

APPENDIX

1. *Basic relationships*

The basic relationships often used in this study are summarized as follows.

$$f(\mathbf{x})*g(\mathbf{x})=g(\mathbf{x})*f(\mathbf{x}). \tag{46}$$

$$f(\mathbf{x})*g(\mathbf{x})*h(\mathbf{x})=\{f(\mathbf{x})*g(\mathbf{x})\}*h(\mathbf{x}) =f(\mathbf{x})*\{g(\mathbf{x})*h(\mathbf{x})\}. \tag{47}$$

$$f(\mathbf{x})*\delta(\mathbf{x}-\mathbf{x}_0)=f(\mathbf{x}-\mathbf{x}_0). \tag{48}$$

$$\exp[-ax^2]*\exp[-bx^2] =\{\pi/(a+b)\}^{1/2}\exp[-abx^2/(a+b)], \tag{49}$$

where $*$ is the one-dimensional convolution, and a, $b>0$.

$$\mathscr{F}[f(\mathbf{x})g(\mathbf{x})]=\mathscr{F}[f(\mathbf{x})]*\mathscr{F}[g(\mathbf{x})], \tag{50}$$

where $*$ is the convolution with respect to $\mathbf{s}$.

$$\mathscr{F}[f(\mathbf{x})*g(\mathbf{x})]=\mathscr{F}[f(\mathbf{x})]\mathscr{F}[g(\mathbf{x})]. \tag{51}$$

$$\mathscr{F}[f(\mathbf{x})*^n]=\{\mathscr{F}[f(\mathbf{x})]\}^n. \tag{52}$$

$$\overline{\mathscr{F}[f(\mathbf{x})]}=\mathscr{F}[f(-\mathbf{x})], \tag{53}$$

where $f(\mathbf{x})$ is a real function and $\overline{\quad}$ stands for the complex conjugate.

$$\mathscr{F}[\delta(\mathbf{x}-\mathbf{x}_0)]=\exp[-2\pi i\,\mathbf{s}\,.\,\mathbf{x}_0]. \tag{54}$$

$$\mathscr{F}(1)=\delta(\mathbf{s}), \tag{55}$$

where $\mathscr{F}$ is the one-dimensional Fourier transform.

$$\mathscr{F}[\exp(-ax^2)]=(\pi/a)^{1/2}\exp[-\pi^2 s^2/a], \tag{56}$$

where $\mathscr{F}$ is the one-dimensional Fourier transform and $a>0$.

$$|\mathscr{F}[f(\mathbf{x})]|\le\int|f(\mathbf{x})|\,\mathrm{d}v_x. \tag{57}$$

$$\int_{-\infty}^{\infty}\exp[-(ax^2+bx+c)]\,\mathrm{d}x =(\pi/a)^{1/2}\exp[(b^2-4ac)/(4a)], \tag{58}$$

where $a>0$.

$$\sin^2[\pi Nh]/\sin^2[\pi h]\simeq\sum_{h_0}N^2\exp[-\pi N^2(h-h_0)^2], \tag{59}$$

where N is an integer.

$$\sin^2[\pi Nh]/(\pi h)^2\simeq N^2\exp[-\pi N^2h^2]. \tag{60}$$

$$1/\{a-\cos(2\pi h)\}\simeq\sum_{h_0}2/(a^2-1) \times\exp(-2\pi(h-h_0)^2/\{(a-1) \times[a-(a^2-1)^{1/2}]\})+1/(a+1), \tag{61}$$

where $a>1$.

$$\mathbf{a}^*=(\mathbf{b}\times\mathbf{c})/\{\mathbf{a}\,.\,(\mathbf{b}\times\mathbf{c})\}. \tag{62}$$

$$\mathbf{a}^*\,.\,\mathbf{a}^*=|\mathbf{b}|^2|\mathbf{c}|^2\sin^2\alpha v^{-2} \tag{63}$$

$$\mathbf{a}^*\,.\,\mathbf{b}^*=|\mathbf{a}||\mathbf{b}||\mathbf{c}|^2v^{-2}(\cos\alpha\cos\beta-\cos\gamma). \tag{64}$$

$$\mathbf{a}^*\,.\,\mathbf{a}=1. \tag{65}$$

$$\mathbf{a}^*\,.\,\mathbf{b}=0. \tag{66}$$

Similar equations to (62)-(66) are valid for $\mathbf{b}^*$ and $\mathbf{c}^*$.

$$v=|\mathbf{a}||\mathbf{b}||\mathbf{c}|\{1-\cos^2\alpha-\cos^2\beta-\cos^2\gamma +2\cos\alpha\cos\beta\cos\gamma\}^{1/2}. \tag{67}$$

2. $|\mathscr{F}(\rho_s)|^2$

Substitution of (4) into (20) and with (54), (51) and (28),

$$\begin{aligned}\mathscr{F}(\rho_s)&\simeq 1+\int\exp[-2\pi i\mathbf{s}\,.\,\mathbf{y}] \times\delta[\mathbf{y}-(\mathbf{a}/3+2\mathbf{b}/3+\mathbf{c}/2)]*D(\mathbf{y})\,\mathrm{d}v_y\\ &=1+\mathscr{F}\{\delta[\mathbf{y}-(\mathbf{a}/3+2\mathbf{b}/3+\mathbf{c}/2)]*D(\mathbf{y})\}\\ &=1+\exp[-2\pi i(h/3+2k/3 +l/2)]R\exp[2\pi i\zeta],\end{aligned}$$

which leads to (25).

3. $|\mathscr{F}(\rho_c)|^2$

Equations (53), (51), (5) and (50) lead to

$$\begin{aligned}|\mathscr{F}(\rho_c)|^2&=\mathscr{F}[\rho_c(\mathbf{x})*\rho_c(-\mathbf{x})]\\ &=\mathscr{F}[N_i(\mathbf{x})]*\mathscr{F}\{\delta(\mathbf{x}) +\sum_{n=1}^{\infty}[\delta(\mathbf{x}-\mathbf{c})*D(\mathbf{x})*D(\mathbf{x})]*^n +\sum_{n=1}^{\infty}[\delta(-\mathbf{x}-\mathbf{c})*D(-\mathbf{x})*D(-\mathbf{x})]*^n\}.\end{aligned}$$

When $R<1$, equations (51)-(54), (28) and (29) give

$$\begin{aligned}&\mathscr{F}\{\delta(\mathbf{x})+\sum_{n=1}^{\infty}[\delta(\mathbf{x}-\mathbf{c})*D(\mathbf{x})*D(\mathbf{x})]*^n +\sum_{n=1}^{\infty}[\delta(-\mathbf{x}-\mathbf{c})*D(-\mathbf{x})*D(-\mathbf{x})]*^n\}\\ &=\sum_{n=0}^{\infty}\{R^2\exp[-2\pi i(l-2\zeta)]\}^n +\sum_{n=0}^{\infty}\{R^2\exp[2\pi i(l-2\zeta)]\}^n-1\\ &=\{1-R^2\exp[-2\pi i(l-2\zeta)]\}^{-1} +\{1-R^2\exp[2\pi i(l-2\zeta)]\}^{-1}-1\\ &=\{1-R^4\}/\{1+R^4-2R^2\cos[2\pi(l-2\zeta)]\}.\end{aligned}$$

On the other hand, from (6) and (55),

$$\mathscr{F}[N_i(\mathbf{x})]=v\delta(h)\delta(k)\sin^2(\pi N_c l)/(\pi l)^2.$$

By using (61), (60), (49) together with the relation

$$\exp[-a(x-x_0)^2]*\exp[-bx^2]$$
$$=\delta(x-x_0)*\{\exp[-ax^2]*\exp[-bx^2]\},$$

we obtain (26), which is also valid for $R=1$.

References

BONART, R., HOSEMANN, R. & MCCULLOUGH, R. L. (1963). *Polymer*, **4**, 199-211.

FISCHER, L. & RULAND, W. (1980). *Colloid Polym. Sci.* **258**, 917-922.

FRANKLIN, R. E. (1951). *Proc. R. Soc. London Ser. A*, **209**, 196-218.

GUENTERT, O. J. & CVIKEVICH, S. (1964). *Carbon*, **1**, 309-313.

HOUSKA, C. R. & WARREN, B. E. (1954). *J. Appl. Phys.* **25**, 1503-1509.

RULAND, W. (1965). *Acta Cryst.* **18**, 992-996.

RULAND, W. (1968). *Chemistry and Physics of Carbon*, Vol. 4. New York: Marcel Dekker.

RULAND, W. & TOMPA, H. (1968). *Acta Cryst.* A**24**, 93-99.

RULAND, W. & TOMPA, H. (1972). *J. Appl. Cryst.* **5**, 225-230.

WARREN, B. E. (1941). *Phys. Rev.* **59**, 693-698.

Acta Cryst. (1988). A**44**, 157-163

The Influence of Texture on the Strain Measured by Diffraction

BY P. PENNING AND C. M. BRAKMAN

Delft University of Technology, Laboratory of Metallurgy, Rotterdamseweg 137, 2628 *AL Delft, The Netherlands*

(*Received* 28 *April* 1987; *accepted* 1 *October* 1987)

Abstract

Strain, as determined by diffraction techniques, is calculated from its constituents. First, the fraction of the crystals that have the proper orientation for diffraction. One degree of freedom is present: the angle of rotation φ_2'' about the scattering vector that the diffracting crystals have in common. The proper orientations, expressed in Euler angles, lie on a line ('trace') in orientation space. The density along the trace is asserted to be known as a Fourier series in φ_2''. Second, the strain in the diffracting crystals. The simplest possible models are discussed: the Voigt and Reuss approximations. The symmetries of the crystal ($m3$ or $m3m$) and of the orientation distribution function (o.d.f.) are taken into account. The dilatation in spacing of the reflecting planes is found as a Fourier series in φ_2'' also. Only the zeroth, first and second harmonic (including phase angles: five parameters) play a part. The diffraction strain is the average over the angle φ_2'' of the dilatation, weighted with the product of the orientation density and the square of the structure factor. For each contributing trace, the corresponding Fourier coefficients have to be multiplied and added to obtain the diffraction strain. The symmetry of the diffraction pole figure is derived.

1. Introduction

The existence of lattice distortions in polycrystalline (metal) samples is well established by means of diffraction techniques. The interpretation of these strains is still the subject of discussion. More specifically, the question whether these strains can be explained by longer-range internal stresses and the character of the relation between the measured strain and the originating stresses is not yet clear. In this paper the influence of texture in the sample is studied. A very simple model is adopted: the material is supposed to be single phase, the orientation distribution function is known and either the stress (Reuss model) or the strain (Voigt model) is uniform over the irradiated volume.* Even in this model the treatment is elaborate because of the many parameters involved. The measured diffraction strain is a weighted average of the dilatation in spacing of the diffracting set of planes. The average is split into its constituents: the volume fraction of the differently oriented grains that diffract, where the texture plays a part, and the strain in these crystals, where the elastic anisotropy is determining. It is shown that texture leads to the observed 'non-linearities' and 'oscillations' in the plots of d_{HKL} *vs* $\sin^2\psi$. Comparison with experiments must show whether the texture is responsible for the entire effect or that the other causes mentioned in the literature (Dölle, 1979; James & Cohen, 1980; Hauk, 1984) play a part also.

2. Experimental procedures to measure diffraction strain

The spacing in the set of reflecting planes (HKL) is determined by diffraction techniques. The mono-

* This implies that any effect of prior plastic deformation leading to a correlation between stress or deformation state and orientation of the grain is not considered.

0108-7673/88/020157-07$03.00